Frustrated magnet for adiabatic demagnetization cooling to milli-Kelvin temperatures

Yoshifumi Tokiwa, Sebastian Bachus, Kavita Kavita, Anton Jesche, Alexander A. Tsirlin, Philipp Gegenwart

Angaben zur Veröffentlichung / Publication details:

Tokiwa, Yoshifumi, Sebastian Bachus, Kavita Kavita, Anton Jesche, Alexander A. Tsirlin, and Philipp Gegenwart. 2021. "Frustrated magnet for adiabatic demagnetization cooling to milli-Kelvin temperatures." Communications Materials 2 (1): 42. https://doi.org/10.1038/s43246-021-00142-1.

communications materials

ARTICLE

https://doi.org/10.1038/s43246-021-00142-1 OPEN

Frustrated magnet for adiabatic demagnetization cooling to milli-Kelvin temperatures

Yoshifumi Tokiwa [1,2✉], Sebastian Bachus[1], Kavita Kavita[1], Anton Jesche [1], Alexander A. Tsirlin[1] & Philipp Gegenwart [1]

Generation of very low temperatures has been crucially important for applications and fundamental research, as low-temperature quantum coherence enables operation of quantum computers and formation of exotic quantum states, such as superfluidity and superconductivity. One of the major techniques to reach milli-Kelvin temperatures is adiabatic demagnetization refrigeration. This method uses almost non-interacting magnetic moments of paramagnetic salts where large distances suppress interactions between the moments. The large spatial separations are facilitated by water molecules, with a drawback of reduced stability of the material. Here, we show that the water-free frustrated magnet $KBaYb(BO_3)_2$ can be ideal for refrigeration, achieving at least 22 mK. Compared to conventional refrigerants, $KBaYb(BO_3)_2$ does not degrade even under high temperatures and ultra-high vacuum. Further, its magnetic frustration and structural randomness enable cooling to temperatures several times lower than the energy scale of magnetic interactions, which is the main limiting factor for the base temperature of conventional refrigerants.

[1] Experimental Physics VI, Center for Electronic Correlations and Magnetism, University of Augsburg, Augsburg, Germany. [2] Advanced Science Research Center, Japan Atomic Energy Agency, Tokai, Ibaraki, Japan. ✉email: ytokiwa@gmail.com

Suppression of thermal fluctuations by lowering temperature gives access to intricate and potentially usable quantum effects. Major discoveries, such as the quantum Hall effect and superfluidity and superconductivity, have been made by explorations of matter close to absolute zero[1,2]. Recently, the development of quantum computers and sensors for dark matter detection rendered low-temperature refrigeration an important technological challenge[3,4]. One of the viable methods for reaching the milli-K (mK) temperature range is adiabatic demagnetization refrigeration (ADR) using paramagnetic salts[5–7]. Its main advantages over the currently dominant technique, ^{3}He–^{4}He dilution refrigeration, are the simple construction of a cooling device and its operation without the usage of expensive ^{3}He. The recent crisis of ^{3}He, which was caused by the increased demand due to the construction of neutron detectors for defense against nuclear terrorism, raised serious concerns about the strong dependence of the current technology on such a scarcely available and ever more expensive gas[8–10]. This triggered renewed interest in ADR, as well as interesting proposals of completely new types of ADR materials[11–19].

The only advantage of ^{3}He–^{4}He dilution refrigeration is its capability of continuous cooling while conventional ADR is a single-shot technique. This makes the ^{3}He–^{4}He dilution refrigeration more commonly used than ADR. However, the situation may change thanks to recent developments of continuous ADR cooling[20,21] and the availability of commercial continuous refrigerators based on ADR[22]. Therefore, ADR has the potential of becoming the main cooling technology already in near future, at least in the mK temperature range.

ADR uses magnetic moments of almost-ideal paramagnets with very weak magnetic interaction $\mathcal{J}$. Because the interaction is weak, magnetic moments are easily aligned by the external magnetic field, causing a reduction of entropy (Fig. 1a, b). Even at zero external magnetic field $H = 0$, magnetic moments of such almost-ideal paramagnets experience some small internal magnetic field produced by adjacent magnetic moments through magnetic interactions. This causes a tiny Zeeman splitting and magnetic order at the same energy scale ($\sim\Delta_0 \sim \mathcal{J}$). Therefore, entropy, which is the driving force of ADR, decreases to zero below the temperature of $T \sim \mathcal{J}$, thus putting a limit on the end temperature $T_f \sim \mathcal{J}$ that can be reached via ADR with this material (Fig. 1b). As indicated by a black horizontal arrow in Fig. 1b, the entropy difference between $H = 0$ and $H \neq 0$ is the key for ADR. While a perfect paramagnet with zero magnetic interactions would be an ideal refrigerant, having maximum entropy at zero fields down to zero temperature, there are always weak but finite interactions in real materials.

For many decades ever since Debye[6] and Giauque[7] independently proposed ADR, water-containing paramagnetic salts have been materials of choice for cooling in the mK range[5,23,24]. In these materials, the interactions are reduced by large distances between the magnetic ions, which are separated by water molecules. However, an abundance of water makes these salts prone to decomposition. They deliquesce in a humid atmosphere and dehydrate in vacuum or upon even mild heating. Therefore, for repeated use without degradation, stable water-free materials with very weak magnetic interactions are desirable. Furthermore, ADR would be certainly beneficial for applications in ultra-high-vacuum (UHV) apparatus, especially in scanning tunneling microscopy and angle-resolved photoemission spectroscopy where the necessity of chamber baking at high temperature and high vacuum for reaching UHV makes the use of current ADR materials essentially impossible. It is, therefore, desirable to find suitable ADR materials without water molecules.

One promising candidate for H_2O-free refrigerant is $KBaYb(BO_3)_2$ with magnetic Yb^{3+} ions. At sufficiently low temperatures, only the lowest Kramers doublet of Yb^{3+} is occupied in this material[25]. In its crystal structure depicted in Fig. 1c, d, YbO_6 octahedra with Yb^{3+} magnetic moments are separated spatially within the *ab*-plane by BO_3 triangles. These negatively charged layers are interspersed along the *c*-axis by the positively charged K^+ and Ba^{2+} ions that occupy the single crystallographic site. The shorter Yb–Yb distances of 5.41 Å within the *ab* plane connect magnetic Yb-ions into a triangular lattice, the feature that already caused interest in this[26,27] and isostructural[28–30] rare-earth borates from the perspective of frustrated magnetism[25]. The interplane Yb–Yb distances are only slightly longer (6.64 Å) and cause additional frustration because adjacent triangular layers are shifted relative to each other, as shown by solid lines in Fig. 1c. Such geometrical frustration may shift the magnetic ordering transition toward lower temperatures or even suppress the magnetic order completely. The distribution of K^+ and Ba^{2+} results in uneven electric fields acting on the magnetic Yb^{3+} ions and may lead to random exchange couplings[25] that are also detrimental for the magnetic ordering. Sizable remaining entropy due to the suppression of the magnetic long-range order facilitates the cooling even below $\sim \mathcal{J}$ (Fig. 1b). Moreover, the presence of soft modes in frustrated magnets amplifies the magnetocaloric effect and further lowers the end temperature of the cooling process[17].

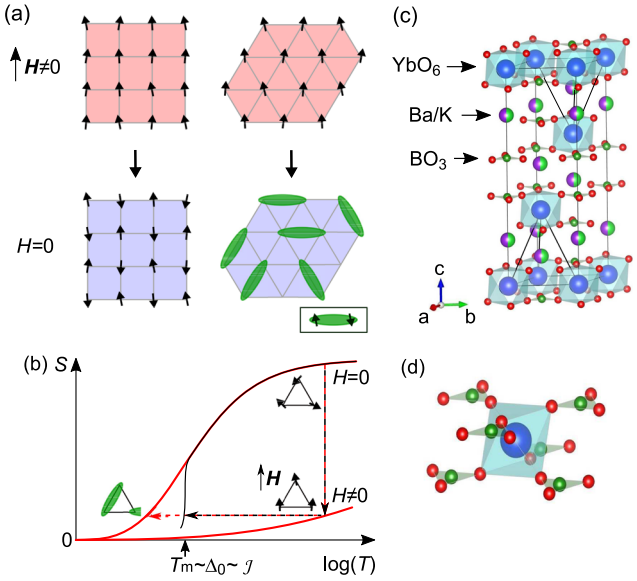

Fig. 1 Adiabatic demagnetization refrigeration. a Cooling process of a conventional paramagnet (left) and a frustrated magnet with impeded magnetic order (right). Green ovals represent singlet pairings in a short-range correlated but long-range disordered state, such as a spin liquid caused by magnetic frustration[25,33] or a random-singlet state caused by structural disorder[34]. **b** Entropy curves at zero and a finite magnetic field as a function of temperature for conventional paramagnets (black) and a system with suppressed magnetic order (red). While the former orders below some temperature T_m around Δ_0, or $\mathcal{J}$, the latter remains disordered down to much lower temperatures where Δ_0 is an energy level splitting at zero external fields because of the internal field caused by magnetic interaction, $\mathcal{J}$. For simplicity, a Schottky-type increase in entropy is assumed. Note, however, that the entropy increase may be much slower in a spin liquid because of its broad energy spectrum. Arrows with red and black dotted lines represent cooling processes for the conventional paramagnets (black) and frustrated magnets (red). **c** Crystal structure of $KBaYb(BO_3)_2$ with triangular layers of the Yb^{3+} ions. Black solid lines highlight the relative displacement of the adjacent triangular layers. **d** YbO_6 octahedron surrounded by the BO_3 triangles.

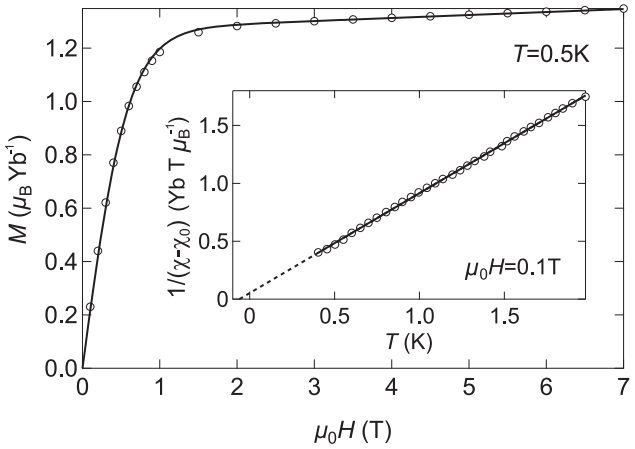

Fig. 2 Magnetic properties of $KBaYb(BO_3)_2$. The field-dependent magnetization of $KBaYb(BO_3)_2$ at 0.5 K. Solid line is a fit to the data with $gJBJ(x) + \chi_0 H$ where g is the g-factor, $J = \frac{1}{2}$ for the lowest Kramers doublet of Yb^{3+}, and B_J is the Brillouin function for $J = \frac{1}{2}$ with $x = (g\mu_B J\mu_0 H) = (k_B T)$. The second term is due to the van Vleck susceptibility χ_0. The fit returns $g = 2.54$ and $\chi_0/\mu_0 = 0.0111\,\mu_B T^{-1}$. The inset shows inverse magnetic susceptibility, $1/(\chi - \chi_0)$ where $\chi = \mu_0 H/M$, measured at 0.1 T. Solid line is a linear fit in the $0.4\,K \le T \le 2.0\,K$ range, resulting in the effective magnetic moment $\mu_{eff} = 2.28\,\mu_B$ and Curie-Weiss temperature $\theta = -60 \pm 2$ mK.

Here, we demonstrate the effective refrigeration with the frustrated magnet $KBaYb(BO_3)_2$ that shows excellent ADR performance on par with conventional water-containing paramagnetic salts and achieves an end temperature T_f of at least 22 mK, starting from a temperature of 2 K at a magnetic field of 5 T. The H_2O-free refrigerant combines several properties that are beneficial for reaching lowest temperatures: the large separation between the magnetic ions, geometrical frustration of residual magnetic interactions, as well as their potential randomness.

Results

Magnetic properties. Magnetization measured down to 0.5 K shows the typical paramagnetic behavior (Fig. 2). Field-dependent magnetization is perfectly described by the Brillouin function augmented by the van Vleck term $\chi_0 H$ that originates from crystal-field excitations. Upon subtracting this van Vleck contribution χ_0 from temperature-dependent susceptibility, one recovers linear behavior in $1/(\chi - \chi_0)$ corresponding to the Curie–Weiss law. The fit returns the effective magnetic moment $\mu_{eff} = 2.28\,\mu_B$ and Curie–Weiss temperature $\theta = -60 \pm 2$ mK. We note that the reduced effective magnetic moment from free Yb^{3+} is due to crystalline electric field effect. We show in Supplementary Fig. 1 that at high temperatures μ_{eff} recovers the free-ion value for Yb^{3+}. The small value of θ indicates that temperatures on the order of 10 mK would be needed to explore cooperative magnetism and frustrated magnetic behavior of $KBaYb(BO_3)_2$, making this material a quite challenging system to study in comparison with $YbMgGaO_4$ and Yb^{3+} delafossites having Curie–Weiss temperatures of several Kelvin[25]. On the other hand, $KBaYb(BO_3)_2$ itself can be used to reach these extremely low temperatures, as we show below.

Specific heat. First hints for the ADR potential of $KBaYb(BO_3)_2$ are found in the magnetic specific heat data $C_m(T)$ that were obtained via subtracting the lattice contribution given by the nonmagnetic reference compound $KBaLu(BO_3)_2$ (Fig. 3a). In zero field, specific heat increases toward lower temperatures and indicates the accumulation of entropy associated with the Kramers doublet of Yb^{3+}. Magnetic field splits this doublet into the

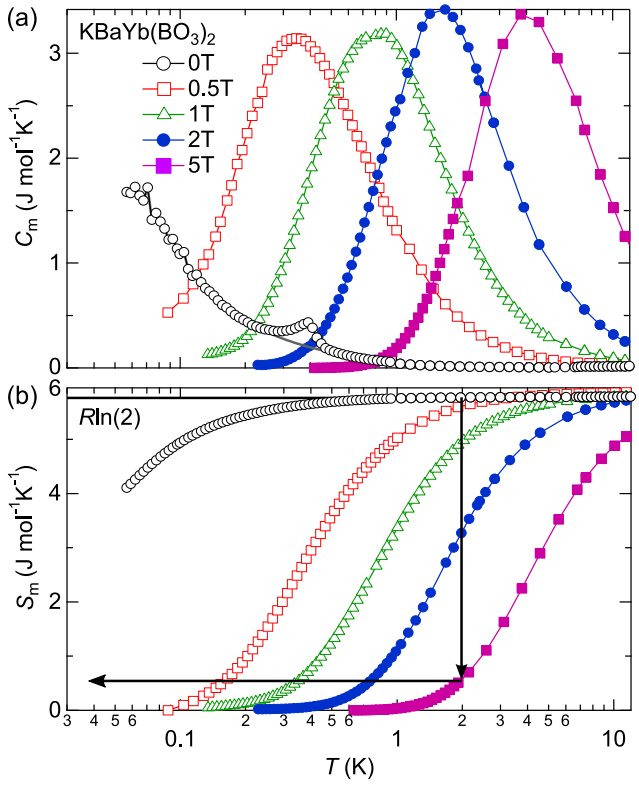

Fig. 3 Estimation of cooling performance. a Low-temperature magnetic heat capacity, C_m of $KBaYb(BO_3)_2$ at several external magnetic fields. Heat capacity of a non-magnetic reference $KBaLu(BO_3)_2$ was subtracted from the raw data as a phonon contribution. **b** Magnetic entropy S_m calculated by integrating C_m/T. In zero field, the entropy is vertically shifted to match $R\ln 2$ expected for the Kramers doublet. Two arrows show the adiabatic demagnetization refrigeration process, starting from $T = 2$ K at $\mu_0 H = 5$ T.

$j_z = +\frac{1}{2}$ and $j_z = -\frac{1}{2}$ levels and causes a Schottky anomaly that shifts toward higher temperatures upon increasing the field. A weak anomaly is seen in the zero-field data around 400 mK, but its nature is probably extrinsic, as it contains only a tiny amount of the magnetic entropy (see Supplementary Fig. 2). Note that a similar anomaly has been reported for isostructural $NaBaYb(BO_3)_2$[28].

By integrating $C_m(T)/T$, we calculate magnetic entropy (Fig. 3b) and observe that already at 0.5 T the full entropy of $R\ln 2$ associated with the lowest Kramers doublet of Yb^{3+} can be recovered above 80 mK. Higher fields shift the entropy toward higher temperatures, so that at 5 T only 10% of $R\ln 2$ is released below 2 K. Therefore, by adiabatic demagnetization of $KBaYb(BO_3)_2$ starting from 2 K and 5 T, one may expect to reach temperatures as low as 30 mK, as shown by arrows in Fig. 3b.

Refrigeration test under the near-adiabatic condition. We test this prediction in the actual cooling experiment that was performed with a 4.02 g pellet containing equal weights of $KBaYb(BO_3)_2$ and silver powder (10–50 μm particle size). Silver improves thermal conductivity within the pellet of insulating $KBaYb(BO_3)_2$. To improve thermal conductance between the particles, we sintered the pressed pellet at 600 °C. The pellet was mounted on a sapphire-plate sample holder, which is held on a plastic frame by four 50 μm thin fishing wires. A resistive RuO_2 thermometer is attached to the pellet with glue. To suppress the thermal conduction from the heat bath, thin superconducting filaments are used as wire leads on the resistive thermometer for temperature measurements. This setup was attached to the cold

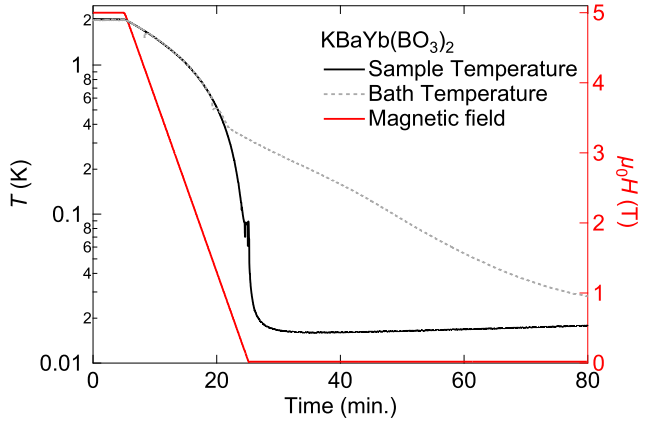

Fig. 4 Refrigeration test under nearly adiabatic conditions. The solid black, solid red, and dotted gray lines are sample temperature (left axis), external magnetic field (right axis), and bath temperature (left axis), respectively. The sample pellet has weak thermal connection to the bath. The bath temperature is controlled to follow the sample temperature to minimize the heat flow. Below about 0.4 K, the bath cannot follow the sample temperature any more because the cooling rate is too fast to follow. The sample holder is in a vacuum chamber with a pressure of ~10^{-6} mbar. The end temperature is 16 mK. Note, however, that the thermometer for this measurement is calibrated down to 22 mK only. Temperature below this limit is obtained by extrapolating the calibration. (See Method and Supplementary Fig. 3).

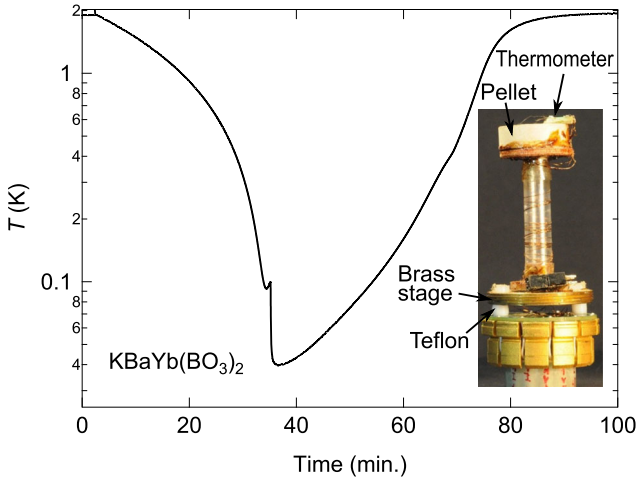

Fig. 5 Cooling performance in the commercial physical property measurement system. The same sample as in Fig. 4 has been used. It is slowly cooled to $T = 2$K at $\mu_0 H = 5$ T through the weak thermal link to the PPMS puck kept at 2 K. Magnetic field is swept from 5 to 0 T with a rate of 0.15 T min^{-1}. The inset shows a photo of the setup with a two-step thermal insulation from the puck (bath). The brass stage is fixed to the puck with two plastic screws having Teflon spacers. The sample pellet is further insulated from the brass stage by inserting a plastic straw. To reduce thermal conductance, 50 μm-diameter 30 cm-long resistive wires (manganin) are used for temperature measurement by the same resistive thermometer as in the test shown in Fig. 4. This setup is shielded from radiation by a standard metallic cap of PPMS.

bath in a vacuum chamber (with the pressure of ~10^{-6} mbar) of the ^{3}He–^{4}He dilution refrigerator.

In order to minimize the heat flow into the sample from the bath, we used a feedback control of the bath temperature (T_b) to follow the sample temperature (T_s). Because the heat flow is $\dot{Q} = \kappa\, \Delta T$ where $\Delta T = T_b - T_s$ and κ is the thermal conductance between the bath and the pellet, minimizing ΔT suppresses $\dot{Q}$ significantly. With the bath temperature of 2 K, the pellet was slowly cooled to 2 K at $\mu_0 H = 5$ T. Then we swept the magnetic field to zero with the 0.25 T min^{-1} rate while giving the feedback control to the bath. As shown in Fig. 4, the pellet is quickly cooled down to less than 22 mK, which is the lowest limit of the thermometer calibration. By extrapolating this calibration to lower temperatures (see Supplementary Fig. 3), we find the end temperature of about 16 mK. A small spike appearing around $T = 80$ mK ($\mu_0 H = 0.1$ T) is probably due to the magnetic flux pinning of the superconducting magnet. After reaching the lowest temperature, the sample warms up slowly due to the heat flow from the surroundings (the bath and radiation). Note that T_b deviates from T_s below 0.4 K. This is because the cooling rate of T_s is too fast for the bath to follow. The large temperature difference indicates a weak thermal conductance between the sample and the bath. Because of the difference, there is finite heat flow into the sample. Therefore, under ideal adiabatic conditions, the end temperature would be even lower than the extrapolated 16 mK.

We note that there is no visible anomaly in sample temperatures other than the spike at 80 mK. A phase transition of second (or first) order would cause a kink (or a local plateau). The absence of such an anomaly confirms the absence of magnetic ordering in $KBaYb(BO_3)_2$ at least down to 22 mK and most likely down to about 16 mK, the temperature several times lower than $|\theta| = 60$ mK. This behavior is in line with the geometrical frustration expected in $KBaYb(BO_3)_2$. Assuming $\theta = -\frac{3}{2}\mathcal{J}$ in a nearest-neighbor triangular antiferromagnet and $T_N/\mathcal{J} \simeq 0.2$ reported for Co-based frustrated materials[25], we estimate $\mathcal{J} \simeq 40$ mK and $T_N \simeq 8$ mK, which would be comparable with the end temperature of 16 mK achieved in our cooling experiment.

Actual refrigeration performance using PPMS. An immediate practical application of an ADR material would be its integration into a commercial physical property measurement system (PPMS) to achieve temperatures below 1.8 K without using ^{3}He. To this end, we constructed a stage where the sample pellet is placed on a tall plastic straw and thermally isolated from the heat bath (Fig. 5). A resistive RuO_2 thermometer is glued on the pellet and connected with thin resistive manganin wires to suppress heat flow. Then the setup is shielded by a metallic cap to reduce thermal radiation from the surroundings. Using the "high-vacuum mode" of the PPMS (pressure below 10^{-4} mbar), we set the bath temperature to 2 K at a magnetic field of 5 T. Then the pellet temperature slowly approaches 2 K by a weak thermal link through the manganin wires and plastic straw. After reaching 2 K, the field is swept to zero with a rate of 0.15 T min^{-1}. The pellet reaches temperatures below 40 mK, with a spike in the sample temperature around 0.1 K due to flux pinning of the superconducting magnet. The pellet warms up back to 2 K in about 50 min by the weak heat conduction. This warming rate is slow enough for data collection of transport properties, such as electrical or Hall resistivity. Although the difference in setup has to be taken into account, the performance of our stage is better than the commercial ADR option for PPMS, which utilizes the paramagnetic salt, chromium potassium alum (CPA), and reaches 100 mK only[31].

Discussion

We conclude that $KBaYb(BO_3)_2$ can be highly efficient in ADR while containing no water molecules and showing excellent stability upon both exposures to air and heating. Key parameters of the ADR materials are compared in Table 1. Figure 3

Table 1 Parameters of adiabatic demagnetization refrigeration materials.

Material	T_m mK	(mag. ion)/Vol. nm^{-3}	S_{GS}	S_{GS}/vol. $mJ\,K^{-1}\,cm^{-3}$
MAS[35]	170	2.8	$R\ln 6$	70
FAA[35]	30	2.1	$R\ln 6$	53
CPA[23]	10	2.2	$R\ln 4$	42
CMN[36]	2	1.7	$R\ln 2$	16
$KBaYb(BO_3)_2$	<22	6.7	$R\ln 2$	64
$YbPt_2Sn$[12]	250	12.9	$R\ln 2$	124
$Yb_3Ga_5O_{12}$[13]	54	13.2	$R\ln 2$	124

T_m is the critical temperature of magnetic order, S_{GS} is the entropy of the ground-state multiplet, and R is the gas constant. The abbreviations stand for MAS: $Mn(NH_4)_2(SO_4)_2{\cdot}6H_2O$ (manganese ammonium sulfate[35]) FAA: $NH_4Fe(SO_4){\cdot}12H_2O$ (ferric ammonium alum[35]) CPA: $KCr(SO_4){\cdot}12H_2O$ (chromium potassium alum[23]) CMN: $Mg_3Ce_2(NO_3)_{12}{\cdot}24H_2O$ (cerium magnesium nitrate[36]).

illustrates that even with the moderate field of 5 T almost all entropy $R\ln 2$ of the lowest Kramers doublet is used for refrigeration. The same is true for conventional paramagnetic salts[5]. Therefore, we list full entropies of the ground state as S_{GS}. From the absolute values of S_{GS} divided by volume, $KBaYb(BO_3)_2$ is clearly competitive with MAS and FAA as "high-temperature" paramagnetic salts that develop magnetic order below T_m of 170 and 30 mK, respectively, and thus cannot cool below these temperatures. The lower-temperature ADR comes at the cost of the higher dilution of the magnetic ions and, therefore, lower S_{GS}/Vol. in CPA and especially CMN. It is in fact natural that the high density of the magnetic moments and low magnetic ordering temperature are unlikely to coexist. Nevertheless, $KBaYb(BO_3)_2$ combines these mutually exclusive properties by virtue of its magnetic frustration and structural randomness that both help to suppress T_m well below the energy scale of magnetic interactions given by $|\theta| = 60$ mK. The material also shows an outstanding density of magnetic ions, 6.7 nm^{-3}, which is much higher than in any of the paramagnetic salts and would allow the design of more compact ADR apparatus. Even higher density has been reported for $YbPt_2Sn$ and $Yb_3Ga_5O_{12}$ that, however, develop magnetic short-range order below 0.25 K and long-range order below 54 mK, respectively, which limits their end temperatures[12,13].

In summary, we demonstrated the H_2O-free refrigerant $KBaYb(BO_3)_2$ with the high entropy/volume ratio and excellent ADR performance of achieving at least 22 mK and possibly temperatures below 16 mK upon demagnetization from $\mu_0 H = 5$ T at 2 K. The absence of water molecules in this refrigerant brings several additional advantages over conventional and commercially used paramagnetic salts. Delicate treatment of these materials is required to avoid degradation and ensure good thermal contact by incorporating wires to the refrigerant pill, which makes production very advanced[21]. With $KBaYb(BO_3)_2$, improving thermal contact is much easier because rough treatments are possible. In the present study, for example, we ground the sample into fine powder and sintered the pressed pellet of a mixture with silver powder at high temperatures. Because of their low stability, water-containing paramagnetic salts have to be sealed air-tight and cannot be heated. The proposed material $KBaYb(BO_3)_2$ is free from all these problems. The chemical stability combined with the excellent cooling performance renders $KBaYb(BO_3)_2$ ideal for ADR applications.

Methods

Sample preparation and characterization. Powder samples of $KBaYb(BO_3)_2$ were prepared by a solid-state reaction of K_2CO_3, $BaCO_3$, Yb_2O_3, and H_3BO_3 taken in stoichiometric amounts, with the 6% excess of H_3BO_3 and 2% excess of K_2CO_3 and $BaCO_3$. The reactants were carefully ground, placed into alumina crucibles, and kept at 200 °C for 6 h to remove absorbed water. They were subsequently annealed at 700 °C for 24 h, re-ground, and re-annealed at 900 °C for another 24 h. All annealing steps were performed in the air. Sintered powders of $KBaYb(BO_3)_2$ were ground and pressed into small pellets with the mass of 18.4 and 2.69 mg used for measurements of magnetic susceptibility and specific heat, respectively.

X-ray powder diffraction pattern was recorded at room temperature using the Empyrean diffractometer from PANalytical (CuK_α radiation, reflection mode). Rietveld refinement (Supplementary Fig. 4) confirmed the formation of $KBaYb(BO_3)_2$ with the lattice parameters $a = 5.41120(2)$ Å, $c = 17.5926(1)$ Å and atomic positions shown in Supplementary Table 1, in good agreement with the earlier report[26]. Several very weak peaks of Yb_2O_3 were detected, corresponding to 0.75(1) wt% of the impurity phase.

Considering that only 0.75(1) wt% of the Yb_2O_3 impurity is contained in the sample, and the magnetic ordering transition of Yb_2O_3 is at 2.3 K[32], we infer that the anomaly should have a different origin. On the other hand, the small amount of entropy suggests that it is unrelated to $KBaYb(BO_3)_2$ itself. The most plausible explanation would be the presence of an amorphous or weakly crystalline impurity that is not seen in X-ray diffraction. Note also that a similar anomaly has been reported for the isostructural compound $NaBaYb(BO_3)_2$[28].

Measurements and tests at low temperatures. Magnetic susceptibility was measured by an MPMS SQUID magnetometer from Quantum Design equipped with a ^{3}He-refrigerator. Measurements of specific heat in the temperature range from 12 K down to 400 mK were performed by using a Quantum Design, PPMS, equipped with a ^{3}He-refrigerator insert. Specific heat measurements of quasi-adiabatic heat pulse method at the lowest temperature down to 50 mK and the tests for ADR with this material have been performed, using a ^{3}He–^{4}He dilution refrigerator and PPMS.

Extrapolation of thermometer calibration. A ruthenium oxide thermometer is used for the tests of ADR with $KBaYb(BO_3)_2$. It is calibrated down to 22 mK. For temperatures below this lower limit, we have used an extrapolation of the calibration to lower temperatures. Supplementary Fig. 3 shows the extrapolation. Since $T^{-1/4}$ for $\ln(R - R_0)$ where R_0 is the resistance at room temperature, is expected for variable-range hopping in semiconductors, we use a linear fit in Supplementary Fig. 3(left) to the low-temperature part of the data for extrapolation.

Data availability

The data that support the findings of this study are available from the corresponding author upon reasonable request.

Received: 28 October 2020; Accepted: 25 February 2021;
Published online: 12 April 2021

References

1. Goerbig, M. O. Electronic properties of graphene in a strong magnetic field. *Rev. Mod. Phys.* **83**, 1193–1243 (2011).
2. Kamerlingh Onnes, H. Akad. Van Wetenschappen. **14**, 113–818 (1911).
3. Zhu, X. et al. Coherent coupling of a superconducting flux qubit to an electron spin ensemble in diamond. *Nature* **478**, 221–224 (2011).
4. Irwin, K. D. An application of electrothermal feedback for high resolution cryogenic particle detection. *Appl. Phys. Lett.* **66**, 1998–2000 (1995).
5. Pobell, F. *Matter and Methods at Low Temperatures* (Springer, 1992).
6. Debye, P. Einige Bemerkungen zur Magnetisierung bei tiefer Temperatur. *Ann. Phys.* **386**, 1154–1160 (1926).
7. Giauque, W. F. A thermodynamic treatment of certain magnetic effects. a proposed method of producing temperatures considerably below 1° absolute. *J. Am. Chem. Soc.* **49**, 1864–1870 (1927).
8. Shea, D. & Morgan, D. *The Helium-3 shortage: supply, demand, and options for congress*. Technical Report R41419 (Congressional Research Service, 2010).
9. Kouzes, R. T. & Ely, J. H. *Status summary of ^{3}He and neutron detection alternatives for homeland security*. Tech. Rep. PNNL-19360 (Pacific Northwest National Laboratory, 2010) http://www.pnl.gov/main/publications/external/technical_reports/PNNL-19360.pdf.
10. Cho, A. Helium-3 shortage could put freeze on low-temperature research. *Science* **326**, 778–779 (2009).
11. Wolf, B. et al. Magnetocaloric effect and magnetic cooling near a field-induced quantum-critical point. *Proc. Natl Acad. Sci. USA* **108**, 6862–6866 (2011).
12. Jang, D. et al. Large magnetocaloric effect and adiabatic demagnetization refrigeration with $YbPt_2Sn$. *Nat. Commun.* **6**, 8680 (2015).
13. Augusto, D. et al. YbGG material for adiabatic demagnetization in the 100 mK-3K range. *Cryogenics* **105**, 103002 (2020).
14. Tokiwa, Y. et al. Super-heavy electron material as metallic refrigerant for adiabatic demagnetization cooling. *Sci. Adv.* **2**, e1600835 (2016).
15. Evangelisti, M. et al. Cryogenic magnetocaloric effect in a ferromagnetic molecular dimer. *Angew. Chem. Int. Ed.* **50**, 6606–6609 (2011).

16. Baniodeh, A. et al. High spin cycles: topping the spin record for a single molecule verging on quantum criticality. *npj Quantum Mater.* **3**, 10 (2018).
17. Zhitomirsky, M. E. Enhanced magnetocaloric effect in frustrated magnets. *Phys. Rev. B* **67**, 104421 (2003).
18. Wolf, B. et al. Magnetic cooling close to a quantum phase transition-the case of $Er_2Ti_2O_7$. *J. Appl. Phys.* **120**, 142112 (2016).
19. Hu, Y. & Du, A. Magnetization behavior and magnetic entropy change of frustrated ising antiferromagnets on two- and three-dimensional lattices. *J. Phys.* **20**, 125225 (2008).
20. Shirron, P. et al. Development of a cryogen-free continuous ADR for the constellation-X" mission. *Cryogenics* **44**, 581–588 (2004).
21. Bartlett, J. et al. Improved performance of an engineering model cryogen free double adiabatic demagnetization refrigerator. *Cryogenics* **50**, 582–590 (2010).
22. kiutra, "Cryogen-free magnetic refrigeration," https://kiutra.com/technology/.
23. Daniels, J. M., Kurti, N. & Simon, FranzEugen The thermal and magnetic properties of chromium potassium alum below 0.1 K. *Proc. R. Soc. Lond. A* **221**, 243–256 (1954).
24. Vilches, O. E. & Wheatley, J. C. Measurements of the specific heats of three magnetic salts at low temperatures. *Phys. Rev.* **148**, 509–516 (1966a).
25. Li, Y., Gegenwart, P. & Tsirlin, A. A. Spin liquids in geometrically perfect triangular antiferromagnets. *J. Phys.* **32**, 224004 (2020).
26. Sanders, M. B., Cevallos, F. A. & Cava, R. J. Magnetism in the $KBaRE(BO_3)_2$ (RE = Sm, Eu, Gd, Tb, Dy, Ho, Er, Tm, Yb, Lu) series: materials with a triangular rare earth lattice. *Mater. Res. Express* **4**, 036102 (2017).
27. Guo, S., Kong, T., Alex Cevallos, F., Stolze, K. & Cava, R. J. Crystal growth, crystal structure and anisotropic magnetic properties of $KBaR(BO_3)_2$ (R = Y, Gd, Tb, Dy, Ho, Tm, Yb, and Lu) triangular lattice materials. *J. Magn. Magn. Mater.* **472**, 104–110 (2019a).
28. Guo, S., Ghasemi, A., Broholm, C. L. & Cava, R. J. Magnetism on ideal triangular lattices in $NaBaYb(BO_3)_2$. *Phys. Rev. Mater.* **3**, 094404 (2019b).
29. Guo, S. et al. Triangular rare-earth lattice materials $RbBaR(BO_3)_2$ (R = Y, Gd-Yb) and comparison to the $KBaR(BO_3)_2$ analogs. *Inorg. Chem.* **58**, 3308–3315 (2019c).
30. Guo, S., Kong, T. & Cava, R. J. $NaBaR(BO_3)_2$ (R = Dy, Ho, Er and Tm): structurally perfect triangular lattice materials with two rare earth layers. *Mater. Res. Express* **6**, 106110 (2019d).
31. Aoki, D. & Flouquet, J. Superconductivity and ferromagnetic quantum criticality in uranium compounds. *J. Phys. Soc. Jpn.* **83**, 061011 (2014).
32. Moon, R. M., Koehler, W. C., Child, H. R. & Raubenheimer, L. J. Magnetic structures of Er_2O_3 and Yb_2O_3. *Phys. Rev.* **176**, 722–731 (1968).
33. Balents, L. Spin liquids in frustrated magnets. *Nature* **464**, 199–208 (2010).
34. Dey, S., Andrade, E. C. & Vojta, M. Destruction of long-range order in noncollinear two-dimensional antiferromagnets by random-bond disorder. *Phys. Rev. B* **101**, 020411(R) (2020).
35. Vilches, O. E. & Wheatley, J. C. Measurements of the specific heats of three magnetic salts at low temperatures. *Phys. Rev.* **148**, 509–516 (1966b).
36. Fisher, R. A., Hornung, E. W., Brodale, G. E. & Giauque, W. F. Magnetothermodynamics of $Ce_2Mg_3(NO_3)_{12} \cdot 24H_2O$. II. The evaluation of absolute temperature and other thermodynamic properties of cmn to 0.6 mK. *J. Chem. Phys.* **58**, 5584–5604 (1973).

Acknowledgements

We thank Andreas Honecker for fruitful discussions and for organizing a very useful and informative workshop on "New perspectives for low-temperature refrigeration with advanced magnetocaloric materials" in 2018. The work in Augsburg was supported by the German Research Foundation (DFG) via Project no. 107745057 (TRR80) and by the Federal Ministry for Education and Research through the Sofja Kovalevskaya Award of Alexander von Humboldt Foundation (AAT). The work in Tokai, Japan was supported by JSPS KAKENHI Grant nos. 20K22338 and 20KK0061.

Author contributions

Y.T., A.A.T. and P.G. conceived and designed the study. Y.T. and S.B. performed the specific heat measurements, the tests using dilution refrigerator and PPMS. K.K. and A.J. performed the magnetic susceptibility measurements. K.K. and A.J. prepared and characterized the samples. Y.T., S.B., A.A.T., and P.G. discussed the results. Y.T. and A.A.T. prepared the paper.

Funding

Open Access funding enabled and organized by Projekt DEAL.

Competing interests

A utility model which covers the fundamental aspects of the publication has been filed in Germany by the University of Augsburg. It is registered under file number 20 2020 002 079. Inventors are Philipp Gegenwart, Alexander A. Tsirlin, and Sebastian Bachus. The remaining authors declare no competing interests.

Additional information

Supplementary information The online version contains supplementary material available at https://doi.org/10.1038/s43246-021-00142-1.

Correspondence and requests for materials should be addressed to Y.T.

Peer review information Primary handling editor: Aldo Isidori.

Reprints and permission information is available at http://www.nature.com/reprints

Publisher's note Springer Nature remains neutral with regard to jurisdictional claims in published maps and institutional affiliations.